nature chemistry

ARTICLES

PUBLISHED ONLINE: 15 AUGUST 2016 | DOI: 10.1038/NCHEM.2588

Mechanically controlled quantum interference in individual π-stacked dimers

Riccardo Frisenda[1†], Vera A. E. C. Janssen[1], Ferdinand C. Grozema[2*], Herre S. J. van der Zant[1*] and Nicolas Renaud[2]

Recent observations of destructive quantum interference in single-molecule junctions confirm the role of quantum effects in the electronic conductance properties of molecular systems. These effects are central to a broad range of chemical and biological processes and may be beneficial for the design of single-molecule electronic components to exploit the intrinsic quantum effects that occur at the molecular scale. Here we show that destructive interference can be turned on or off within the same molecular system by mechanically controlling its conformation. Using a combination of *ab initio* calculations and single-molecule conductance measurements, we demonstrate the existence of a quasiperiodic destructive quantum-interference pattern along the breaking traces of π-stacked molecular dimers. The results demonstrate that it is possible to control the molecular conductance over more than one order of magnitude and with a sub-ångström resolution by exploiting the subtle structure–property relationship of π-stacked dimers.

Charge transport across non-covalently bonded molecular fragments is a crucial process in chemistry, biology and materials science. For example, the propagation of charge along π-stacked assemblies plays an important role in the oxidative damage and repair of DNA[1,2], participates in the early stages of charge separation in the photosynthesis apparatus[3,4] and controls the efficiency of organic materials for electronic applications[5,6]. The efficiency of charge transport through π-stacked molecules is controlled by electronic coupling between neighbouring molecules and therefore depends in an intricate way on the distance and respective orientation of the π systems[7–9]. Although the impact of such molecular packing on charge mobility is well understood for organic crystals[5], only a few experiments have probed the structure–property relationship of π-stacked dimers at the single-molecule level[10–14]. A better understanding of coherent charge transport through π-stacked molecules could therefore be beneficial to the engineering of new materials and may also help to understand fundamental charge-transfer processes in chemistry.

In this contribution, we studied charge transport through π-stacked molecules at the single-molecule level with the mechanically controlled break junction (MCBJ) technique[15]. In the experiment, a π-stacked dimer bridges two lithographically defined metallic electrodes[16,17] that are progressively moved away from each other with sub-ångström control. The motion of the electrodes can be used to manipulate the dimer conformation by slowly separating the two monomers. The current that passes through the molecular structure is measured continuously during the dimer separation by the application of a small bias voltage across the junction. The experiments reveal the presence of pronounced conductance drops when the two π systems slide over each other. A higher-order statistical analysis of the experimental data, guided by electronic structure calculations, leads to the conclusion that these drops result from destructive quantum-interference effects[18–20]. The results therefore show that such effects can be turned on and off within the same system by mechanically controlling its conformation. The large on/off conductance ratio can be used to design single-molecule electronic[12,20–23] or thermoelectric[11] components to exploit the quantum effects that occur at the molecular scale.

Results and discussion

Theory. The molecules studied in this work are shown in Fig. 1a. They consist of an oligo-phenylene-ethynylene (OPE3) π-conjugated molecule, with either one (S–OPE3) or two (S–OPE3–S) thiol anchoring groups. Previous studies have demonstrated that single S–OPE3–S molecules reproducibly form molecular junctions in which a single molecule bridges the two electrodes[24]. In contrast, S–OPE3 only contains a single anchoring group and therefore two molecules are required to form a π-stacked dimer and to create a mechanically stable electronic connection between the two electrodes[10,13], as illustrated in Fig. 1b.

The electronic transport properties of S–OPE3 dimers and S–OPE3–S were calculated at the density functional level of theory (DFT) using the Landauer formalism[25] in the wide-band-limit approximation[26]. The main results of these calculations are summarized in Fig. 1c. In the case of S–OPE3–S molecules, *ab initio* calculations at the optimized junction geometry yield a conductance of $2 \times 10^{-5}\ G_0$, where $G_0 = 77\ \mu S$ is the quantum of conductance. In the case of a π-stacked S–OPE3 dimer, the conductance was calculated as a function of displacement of the two molecules with respect to each other (see Fig. 1b). As shown in Fig. 1c, the resulting zero-bias conductance strongly depends on the stacking geometry of the molecules, with very sharp quasiperiodic conductance drops over several orders of magnitude and separated by 0.21–0.25 nm. These conductance drops can be traced back to destructive quantum-interference effects that occur exactly at the Fermi energy of the electrodes for specific dimer conformations (see Supplementary Figs 1 and 2). Additionally, transport calculations combined with molecular dynamics simulations clearly demonstrate that these pronounced modulations of the conductance that result from quantum interference are still statistically detectable, even at room temperature (Supplementary Fig. 10).

[1]Kavli Institute of Nanoscience, Delft University of Technology, Lorentzweg 1, 2628 CJ Delft, The Netherlands. [2]Department of Chemical Engineering, Delft University of Technology, Julianalaan 136, 2628 BL Delft, The Netherlands. [†]Present address: Instituto Madrileño de Estudios Avanzados en Nanociencia (IMDEA-nanociencia), Campus de Cantoblanco, E-28049 Madrid, Spain. *e-mail: f.c.grozema@tudelft.nl; h.s.j.vanderzant@tudelft.nl

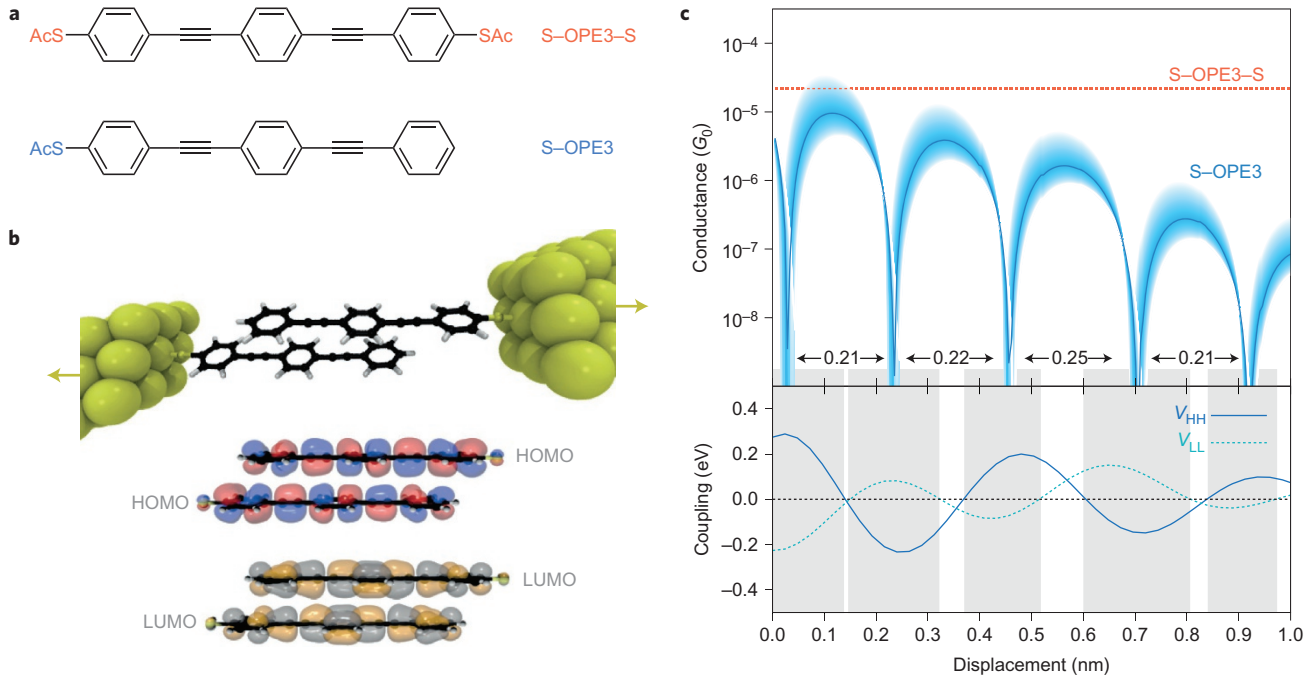

Figure 1 | Simulations of the electronic transport properties of S-OPE3 and S-OPE3-S. a, Chemical structures of the two molecules studied in this Article, which feature acetyl-protected thiol groups (SAc). **b**, Representation of the two electrodes in the break junction connected by a π-stacked dimer. Fragment molecular orbitals of both dimers are shown. **c**, The top panel shows the conductance of S-OPE3 in the wide-band-limit approximation calculated at the Fermi energy (plain blue line). The shaded area around it corresponds to a variation of the Fermi energy of ±0.5 eV. The horizontal dashed line marks the conductance of S-OPE3-S. The bottom panel shows intermolecular couplings between the HOMO (blue line, V_{HH}) and LUMO (dashed blue line, V_{LL}) fragment molecular orbitals of S-OPE3. The drops in conductance observed for S-OPE3 result from quantum-interference effects and occur when the intermolecular couplings have opposite signs.

These modulations of the conductance are preserved when the band alignment shifts between the electrodes and the molecules, as illustrated by the blue-shaded area in Fig. 1c. However, this effect can be blurred significantly if one of the two molecules interacts with both electrodes, as illustrated in Supplementary Fig. 28.

Our calculations show that the couplings between the frontier molecular orbitals play a crucial role in these quantum-interference effects. A representation of these orbitals, that is, the highest occupied molecular orbital (HOMO) and the lowest unoccupied molecular orbital (LUMO), on each monomer is shown in Fig. 1b. The variations of the electronic coupling, V_{HH}, between the HOMO of one molecule and the HOMO of the other, as well as the LUMO–LUMO coupling (V_{LL}), are shown in Fig. 1c. Both vary strongly with the stacking geometry of the dimer, taking alternatingly positive and negative values. This alternation can be understood from the structure of the molecular orbitals (Fig. 1b). Depending on the relative displacement of the two molecules, the overlap of their HOMOs can either be positive, which leads to a negative coupling, or negative, which leads to a positive coupling. This argument also holds for the two LUMOs.

By comparing the two graphs in Fig. 1c, we can see that the sharp drops observed in the conductance of the S–OPE3 dimer occur within the regions in which the HOMO–HOMO and LUMO–LUMO electronic couplings have opposite sign (grey-shaded area in Fig. 1c). As seen in Supplementary Fig. 1, a destructive interference pattern is always present somewhere in the gap of the junction when the couplings have opposite signs. The study of a model four-level quantum system, reported in Supplementary Fig. 5, confirms a direct link between the opposite sign of the intermolecular electronic couplings and the presence of destructive quantum interference. As the values of these couplings are dictated by the overlap between the molecular orbitals, the observation of a quasiperiodic destructive interference pattern constitutes a unique way to probe the structure and phase of the fragment orbitals. As a consequence, this effect is very general and can be observed with any dimers of π-conjugated systems, albeit with different periodicities (see, for example, Supplementary Fig. 11). This effect can even be generalized to more-complex systems, such as the trimers and tetramers represented in Supplementary Figs 25–27.

Break-junction experiments. Measurements of the conductance through S–OPE3 dimers and S–OPE3–S molecules were performed using the MCBJ technique[27]. In this technique, a nanometre-size gap in a lithographically defined gold nanowire is repeatedly opened and closed in the presence of molecules that can be trapped between the electrodes. The continuous measurement of the molecular conductance as the electrodes are displaced results in a so-called breaking trace.

We measured 1,878 breaking traces for S–OPE3 and 1,000 for S–OPE3–S. The breaking speed chosen was 3–10 pm s^{-1}, about two orders of magnitude slower than in the usual experiments, to obtain detailed information of the conductance traces. Representative traces are shown in Fig. 2a. For both S–OPE3 and S–OPE3–S, stable conductance plateaus were observed after opening the nanogap, which indicates the formation of a single-molecule junction. The breaking traces of S–OPE3 are generally longer than those of S–OPE3–S and exhibit a more-complex structure with multiple conductance plateaus and pronounced conductance drops. These drops show a reduction of the conductance by two orders of magnitude on displacement of the electrodes by a few hundred picometres (inset of Fig. 2a). As seen in Fig. 2a, the breaking traces end abruptly when the contact between the two electrodes is disrupted because of either the detachment of one molecule from the electrode or the rupture of the π stacking between two

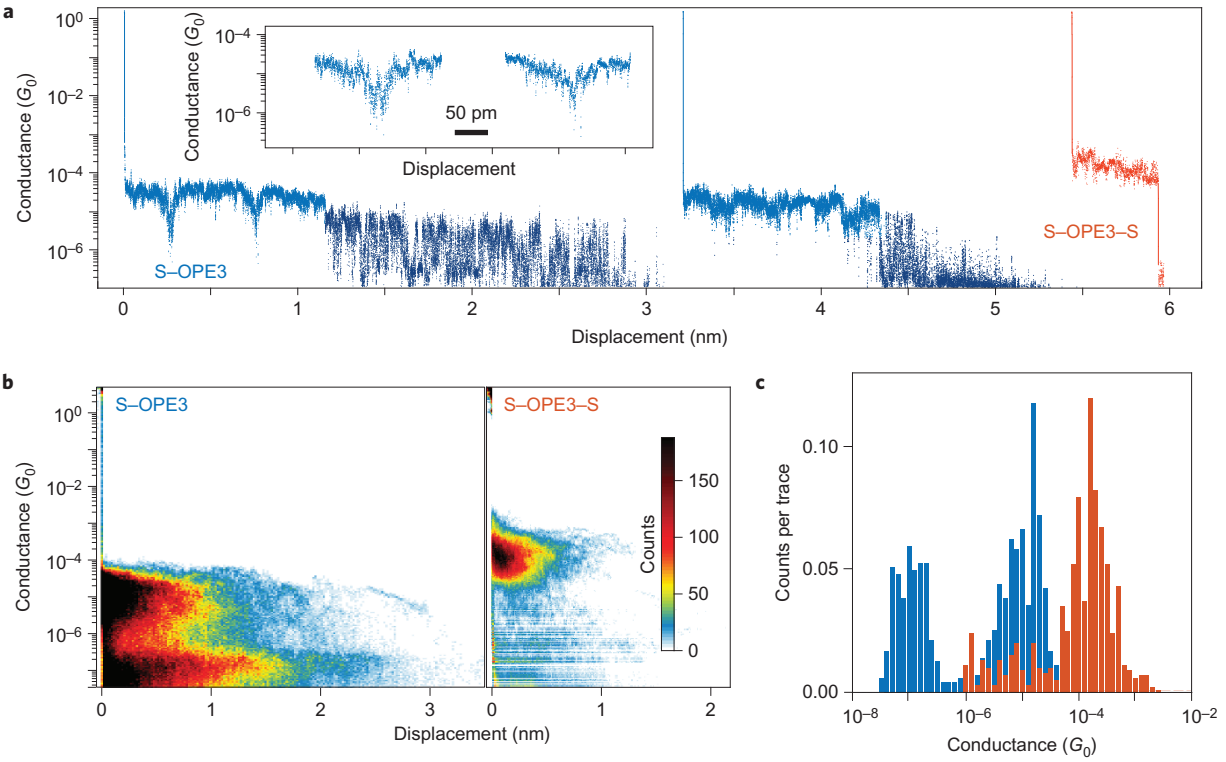

Figure 2 | Conductance analysis of S-OPE3 π-stacked dimers. a, Examples of breaking traces measured in the presence of S-OPE3 (blue) and S-OPE3-S (red). The bias voltage is 100 mV and the electrode-separation speed is 3 pm s^{-1} in the first case and 10 pm s^{-1} in the second case. **b**, 2D conductance–displacement histogram of S-OPE3 and S-OPE3-S built from 1,878 and 1,000 consecutive traces, respectively. A small number of counts at low conductance values were also observed for S-OPE3-S; these may be the result of dimers formed by these molecules, albeit with a low probability. **c**, Conductance histograms built from the mean conductance of each plateau found from a single-trace analysis. The inset in **a** shows a zoom-in on the drops observed in the monothiol molecule, which are attributed to the quantum-interference effects.

monomers. At this point, the motion of the electrodes is reversed until the gap in the gold wire is completely closed and a new opening/closing cycle starts.

To obtain a representative picture of the conductance properties of both molecules, we constructed two-dimensional (2D) conductance–displacement histograms from the full data sets of breaking traces. These histograms, shown in Fig. 2b, indicate how often a certain combination of conductance and displacement occurs. Clear differences are observed in the histograms for the two molecules. For S–OPE3–S, a single region of high counts is observed that extends to ~0.5 nm near 10^{-4} G_0. This conductance value is comparable to those of previous studies of the S–OPE3–S single-molecule conductance[24] and to our theoretical calculations. In contrast, the conductance histogram for S–OPE3 exhibits two characteristic regions of high probability, one with a high-conductance state at around 10^{-5} G_0 and a lower one at around 10^{-7} G_0. These two regions extend for about 1.0 nm and 1.7 nm, respectively. A few traces even extend up to 3.5 nm, much longer than the length of a single S–OPE3 molecule (1.8 nm). A similar structure, which shows two preferential values of the dimer conductance, was also observed in our combined molecular dynamics/transport calculations for S–OPE3 dimers (Supplementary Fig. 10). Additionally, the measured values of the zero-bias conductance are in good agreement with our DFT simulations, which include explicit gold clusters to model the electrodes (Supplementary Figs 2 and 4).

The marked differences between the two histograms constitute a strong indication that fundamentally different molecular structures are probed in the presence of S–OPE3 and S–OPE3–S. In addition, the long traces observed for S–OPE3, which extend up to about twice the length of the single molecules, strongly suggest that π-stacked dimers are responsible for the conductance in these experiments. The double-plateau structure observed both experimentally and theoretically indicates the presence of at least two preferential intermolecular conformations of the two molecules, each with a specific conductance value.

Single-trace statistical analysis. Although the conductance histograms reported in Fig. 2b give statistical information across the full data set, they provide little insight into conductance variations along individual breaking traces[28]. To extract this information from our experimental results, we performed an extensive statistical analysis of the single traces. We first identified the different conductance plateaus along the breaking traces of both molecules and computed the mean value and standard deviation of their conductance level as well as their total length. Histograms of these mean conductance values are reported in Fig. 2c. Scatter plots of the plateau lengths and standard deviations of their conductance level are plotted versus their mean conductance values in Fig. 3a,b, respectively.

This analysis confirms that the breaking traces of S–OPE3–S mainly contain short plateaus with an average length of 0.29 nm and a mean value of conductance of 2×10^{-4} G_0. The length of 0.29 nm indicates that, in contrast to junctions probed in fast-breaking experiments, junctions with slow breaking speeds do not extend over their full length and premature molecule detachment from the electrodes occurs. In contrast, the plateaus of S–OPE3 are clearly separated into two groups. One group presents a conductance value of 1×10^{-5} G_0 and a standard deviation of 0.41 decades, whereas the other shows a lower mean value of 2×10^{-7} G_0 with a larger standard deviation of 0.65 decades.

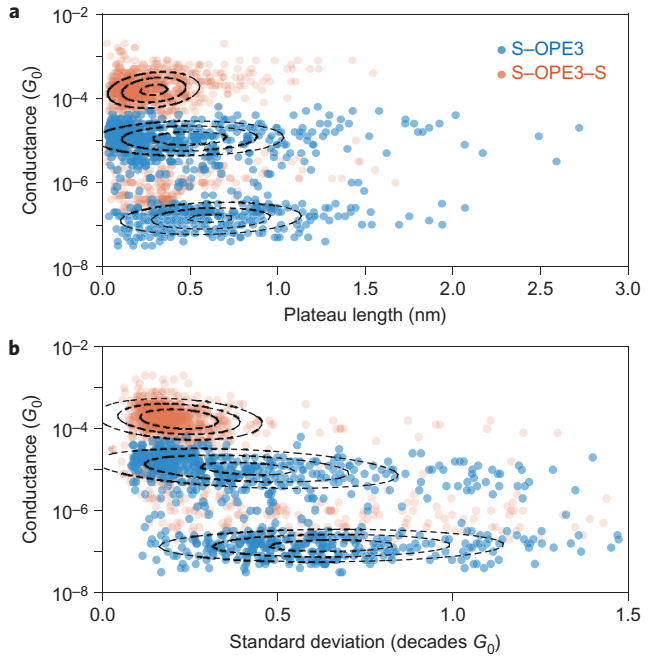

Figure 3 | Statistical analysis of the conductance plateaus. a,**b**, Scatter plots of the plateau length (**a**) and of the standard deviation (**b**) versus the conductance from the analysis of all the plateaus measured for S-OPE3 (blue) and S-OPE3-S (red). Each dot represents a single-conductance plateau extracted from the breaking traces. The dashed lines represent the contour level of bivariate normal distributions. One single bivariate normal peak is sufficient to fit the S-OPE3-S distribution, whereas two peaks are needed for S-OPE3. This analysis clearly shows that different molecular structures are probed in the presence of S-OPE3 or S-OPE3-S.

The average lengths of the plateaus in the two groups are 0.47 and 0.62 nm, respectively. These results again point to the existence of two π-stacked conformations of S–OPE3 with different binding energies. This is consistent with our theoretical calculations that show two local minima of the dimer binding energy separated by about 0.7 nm (Supplementary Fig. 6). The slight difference between the experimental results and theoretical predictions of the plateau length may arise from the diffusion of the molecules at the surface of the electrodes. The large standard deviation observed in the second conductance plateau can be explained by the small binding energy of weakly overlapping dimers.

As mentioned above, sharp conductance drops, highlighted in Fig. 2a, are observed for the breaking traces of S–OPE3. These conductance drops occur almost exclusively in the presence of S–OPE3 and hence appear to be characteristic of π-stacked dimers. To determine whether these drops result from quantum-interference effects, the distances between consecutive drops were extracted from our experimental results and compared with our theoretical prediction of 0.21–0.25 nm. Given the low standard deviation of their conductance level, the high-conductance plateaus of 132 S–OPE3 traces were considered (Supplementary Fig. 20). A higher-order statistical analysis of single breaking traces (Supplementary Fig. 21), adapted from the detection techniques developed for biological signals[29], was implemented to detect the sharp conductance drops automatically (see Supplementary Section VI for more details). The position and depth of the drops were then used to compute the distribution of drop-to-drop distances in the experimental data. Representative examples of this analysis are given in Fig. 4a for four different breaking traces of S–OPE3. The same analysis was also performed on 259 breaking traces of S–OPE3–S for comparison (Supplementary Fig. 24).

The histograms of the drop-to-drop distance obtained for both molecules are shown in Fig. 4b. As seen in this figure, our statistical analysis clearly demonstrates that the conductance drops are predominantly found in S–OPE3. Although some drops were also found along the breaking traces of S–OPE3–S, they are much less pronounced than those found for S–OPE3 molecules (see Supplementary Fig. 24). The statistical analysis of single traces further reveals that the drop-to-drop distance distribution for the S–OPE3 breaking traces is not random. A kernel density-estimation fitting of the distribution, shown as a full black line in Fig. 4b, leads to two peaks located at 0.05 and 0.27 nm, respectively. As demonstrated in Supplementary Section IV-D, the first peak can be attributed to an intrinsic limitation of the detection algorithm. This is confirmed by the appearance of a similar peak in the distribution of the drop-to-drop distances obtained for theoretical traces in the presence of noise, as shown in the inset of Fig. 4b. Interestingly, the position of the second peak in the experimental distribution is close to the theoretical prediction of 0.21–0.25 nm. Considering that several factors may influence the drop-to-drop distance, we find the agreement between the theoretical prediction and the experimental detection satisfactory. These factors include uncertainties related to the theoretical treatment (level of theory, presence of gold clusters, position of the Fermi energy), but also to physical issues, such as the possibility that a bound molecule moves to a different position on the surface of the gold electrode during the recording of the breaking trace. The latter can lead to an apparent increase or decrease in the distance between consecutive conductance drops.

Finally, a wide range of mechanisms can also induce a significant reduction of the conductance. This is, for example, the case for an increase of the π-stacking distance between the two monomers or the deviation of one molecule from the axis of the junction (see Supplementary Fig. 7). However, as argued in Supplementary Section II, the conductance drops induced by these mechanisms are expected to occur at random places, in contrast with the distribution shown in Fig. 4b. The statistical analysis developed in this Article consequently allows these undesirable conductance drops to be distinguished from those induced by quantum-interference effects.

We present here a combined theoretical and experimental study of electronic transport across π-stacked dimers. The theoretical analysis reveals the presence of quasiperiodic conductance drops along breaking traces of π-stacked dimers. These drops are the result of the destructive quantum interference that occurs when the electronic couplings between the frontier molecular orbitals of the two monomers exhibit opposite signs. As a consequence, the periodicity of the drops is dictated by the structure and phase of the frontier molecular orbitals and does not correspond to the distance between benzene rings. Using a MCBJ experiment, we measured the electronic conductance of molecular π-stacked dimers as we slowly pulled the stacked molecules apart. Large conductance drops were recorded in the breaking traces. A higher-order statistical analysis of the experimental results shows a striking resemblance with the theoretical predictions. The results thus demonstrate the possibility to control molecular conductance over a few orders of magnitude and with sub-ångström resolution by exploiting the subtle structure/property relationship of π-stacked systems. This effect is not limited to the specific molecular structure studied here and a similar behaviour is expected for a large class of molecules. The future study of mechanically controlled quantum interference in π-stacked systems might be facilitated by exploiting specific molecule–molecule interactions that increase the binding energy between them, or by the use of organic cages to encapsulate the monomers partially.

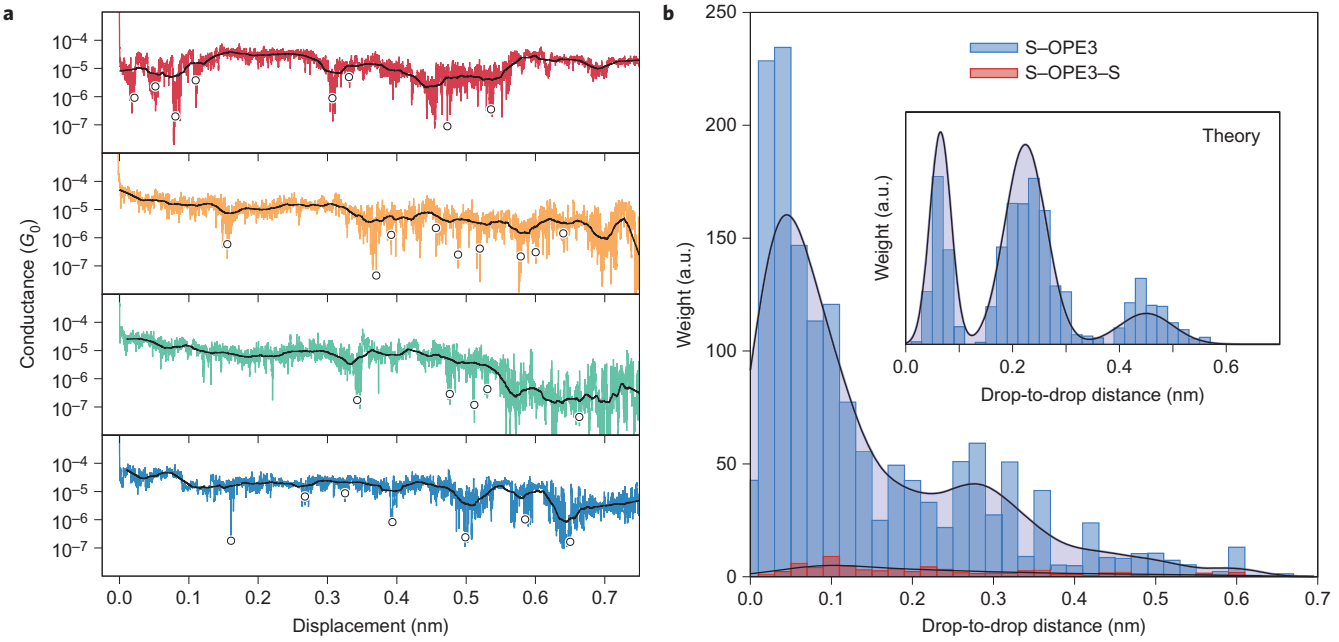

Figure 4 | Statistical analysis of the conductance drops observed in single traces. a, Automatic detection of the conductance drops on a few conduction traces of S–OPE3. The circles mark the conductance drops automatically identified by our algorithm. **b**, Histograms of the weighted drop-to-drop distance obtained from the statistical analysis, performed with 131 traces of S–OPE3 and 259 traces of S–OPE3–S. The black lines show a kernel density-estimation fitting of the distribution. The inset shows the histogram obtained for the theoretical traces of S–OPE3. The analysis shows that the consecutive conductance drops observed experimentally are separated by 0.27 nm, in agreement with theory.

Methods

Simulations. Calculations of the electronic structure were performed at the DFT level of theory using the Amsterdam Density Functional (ADF) package[30]. A double-zeta basis set with polarization was used in combination with the M06-2X functional. The transport calculations in the wide-band limit were made using a home-built program. The electronic-coupling matrix elements were calculated within the ADF package by using the orbitals of the two monomers as basis and by extracting the off-diagonal elements of the Fock matrix[31]. The MD + Transport calculations were performed with a modified version of the TransPull program (https://nanohub.org/resources/11739 (2014)). Explicit frozen gold clusters were considered in these calculations to simulate the bulk electrodes. A detailed discussion of the theoretical methods used here is given in Supplementary Section I.

MCBJ experiments. In the MCBJ experiment, a lithographically fabricated nanoscale gold wire was patterned on a flexible substrate. Electrodes were first characterized without molecules to ensure that they were clean and that they were well aligned (in which case a clear peak at 1 G_0 is observed, indicative of atomically sharp electrodes). After this, a droplet of the solution that contained the molecules (1 mM in dichloromethane) was deposited on the electrodes; after evaporation of the solvent, the measurements were performed in air at room temperature. More details are given in Supplementary Section V-B, and a detailed description of this technique has been given previously[32]. We investigated the low-bias conductance of the two OPE3 molecules at a bias of 100 mV using a low pulling speed of the electrodes of 3 pm s^{-1} in the case of S–OPE3 and 10 pm s^{-1} for S–OPE3–S. This slow pulling speed, in combination with the stability of the MCBJ technique, enabled us to acquire sufficient amounts of data points per breaking trace to facilitate further statistical analysis. All the experiments were performed at room temperature. Similar conductance experiments with S–OPE3 were carried out at lower temperatures ($T = 77$ K and $T = 195$ K), but π-stacked dimer configurations were only observed at room temperature (Supplementary Section V-C). We measured a total of 1,878 conductance breaking traces in the presence of S–OPE3 and 1,000 with S–OPE3–S. The molecular-junction formation yield was 25% in the S–OPE3 case and 90% for S–OPE3–S, which corresponds to 469 molecular junctions in the first case and 901 in the second case.

Analysis of the plateau length. To analyse the plateau lengths and standard deviations we first computed the conductance histogram of each individual breaking trace. We then located the different peaks of this distribution and their half-width at half-maximum (HWHM). After denoising and decimation of the breaking trace, we located the regions in which the conductance signal was within two HWHM around the centre of the conductance peak. We then identified the different plateaus in the original trace and extracted their length and the standard deviation of the conductance. We checked for the algorithm consistency and robustness and found that most of the traces were well analysed; in the few cases of error we corrected the entries manually.

Statistical analysis of conductance drops. We carefully selected 132 traces among the full data set of S–OPE3 breaking traces. As illustrated in Supplementary Fig. 20, these traces were selected based on their total length, number of plateaus and signal-to-noise ratio. The identification of conductance drops along these individual traces was performed via the detection algorithm outlined in Supplementary Fig. 21. This algorithm is based on the stationary wavelet transform of the baseline-corrected breaking traces. The wavelet coefficients were then subjected to a two-stage kurtosis denoising[29] to isolate the drops from the noise regions. Bursts of the cumulative denoised trace were then detected using an infinite hidden Markov chain[33] to identify unique conductance drops. The weighted distribution of the drop-to-drop distance was then computed via the position and depth of each individual drop. The continuous probability function of the drop-to-drop distance distributions was obtained via a kernel density-estimation fitting. Our detection method proved to be robust with respect to various parameters involved in our algorithm, as illustrated in Supplementary Fig. 22.

Data availability. Supplementary Information gives the electronic transport calculations for S–OPE3, S–OPE3–S and the model system, calculations of the dimer-binding energy and associated transport properties, combined molecular dynamics and electronic transport calculations, other example of molecular structures that show mechanically controlled quantum-interference effects, experimental details and the statistical analysis of the conductance drops.

Received 1 February 2016; accepted 1 July 2016; published online 15 August 2016

References

1. Núñez, M. E., Hall, D. B. & Barton, J. K. Long-range oxidative damage to DNA: effects of distance and sequence. *Chem. Biol.* **6,** 85–97 (1999).
2. Merino, E. J., Boal, A. K. & Barton, J. K. Biological contexts for DNA charge transport chemistry. *Curr. Opin. Chem. Biol.* **12,** 229–237 (2008).
3. Brettel, K. & Leibl, W. Electron transfer in photosystem I. *Biochim. Biophys. Acta* **1507,** 100–114 (2001).
4. Wasielewski, M. R. Photoinduced electron transfer in supramolecular systems for artificial photosynthesis. *Chem. Rev.* **92,** 435–461 (1992).
5. Coropceanu, V. *et al.* Charge transport in organic semiconductors. *Chem. Rev.* **107,** 926–952 (2007).
6. Sirringhaus, H. *et al.* Two-dimensional charge transport in self-organized, high-mobility conjugated polymers. *Nature* **401,** 685–688 (1999).

7. Yi, Y., Coropceanu, V. & Bredas, J.-L. A comparative theoretical study of exciton-dissociation and charge-recombination processes in oligothiophene/fullerene and oligothiophene/perylenediimide complexes for organic solar cells. *J. Mater. Chem.* **21,** 1479–1486 (2011).
8. Solomon, G. C., Herrmann, C., Vura-Weis, J., Wasielewski, M. R. & Ratner, M. A. The chameleonic nature of electron transport through π-stacked systems. *J. Am. Chem. Soc.* **132,** 7887–7889 (2010).
9. Delgado, M. C. R., Kim, E.-G., da Silva Filho, D. A. & Bredas, J.-L. Tuning the charge-transport parameters of perylene diimide single crystals via end and/or core functionalization: a density functional theory investigation. *J. Am. Chem. Soc.* **132,** 3375–3387 (2010).
10. Wu, S. *et al.* Molecular junctions based on aromatic coupling. *Nature Nanotech.* **3,** 569–574 (2008).
11. González, M. T. *et al.* Break-junction experiments on acetyl-protected conjugated dithiols under different environmental conditions. *J. Phys. Chem. C* **115,** 17973–17978 (2011).
12. Fujii, S. *et al.* Rectifying electron-transport properties through stacks of aromatic molecules inserted into a self-assembled cage. *J. Am. Chem. Soc.* **137,** 5939–5947 (2015).
13. Martín, S. *et al.* Identifying diversity in nanoscale electrical break junctions. *J. Am. Chem. Soc.* **132,** 9157–9164 (2010).
14. Batra, A. *et al.* Quantifying through-space charge transfer dynamics in π-coupled molecular systems. *Nature Commun.* **3,** 1086 (2012).
15. Tao, N. J. Electron transport in molecular junctions. *Nature Nanotech.* **1,** 173–181 (2006).
16. Li, Q. & Solomon, G. C. Exploring coherent transport through π-stacked systems for molecular electronic devices. *Faraday Discuss.* **174,** 21–35 (2014).
17. Li-Li, L., Xiu-Neng, S., Yi, L. & Chuan-Kui, W. Formation and electronic transport properties of bimolecular junctions based on aromatic coupling. *J. Phys Condens. Matter* **22,** 325102 (2010).
18. Solomon, G. C. *et al.* Quantum interference in acyclic systems: conductance of cross-conjugated molecules. *J. Am. Chem. Soc.* **130,** 17301–17308 (2008).
19. Guedon, C. M. *et al.* Observation of quantum interference in molecular charge transport. *Nature Nanotech.* **7,** 305–309 (2012).
20. Sautet, P. & Joachim, C. Electronic interference produced by a benzene embedded in a polyacetylene chain. *Chem. Phys. Lett.* **153,** 511–516 (1988).
21. Stafford, C. A., Cardamone, D. M. & Mazumdar, S. The quantum interference effect transistor. *Nanotechnology* **18,** 42014 (2007).
22. Baer, R. & Neuhauser, D. Phase coherent electronics: a molecular switch based on quantum interference. *J. Am. Chem. Soc.* **124,** 4200–4201 (2002).
23. Perrin, M. *et al.* Large negative differential conductance in single-molecule break junctions. *Nature Nanotech.* **9,** 830–834 (2014).
24. Frisenda, R. *et al.* Electrical properties and mechanical stability of anchoring groups for single-molecule electronics. *Beilstein J. Nanotechnol.* **6,** 1558–1567 (2015).
25. Cuevas, J. C. & Scheer, E. *Molecular Electronics: An Introduction to Theory and Experiment* (World Scientific, 2010).
26. Verzijl, C. J. O., Seldenthuis, J. S. & Thijssen, J. M. Applicability of the wide-band limit in DFT-based molecular transport calculations. *J. Chem. Phys.* **138,** 094102 (2013).
27. He, J. *et al.* Measuring single molecule conductance with break junctions. *Faraday Discuss.* **131,** 145–154 (2006).
28. Frisenda, R., Perrin, M. L., Valkenier, H., Hummelen, J. C. & van der Zant, H. S. J. Statistical analysis of single-molecule breaking traces. *Phys. Status Solidi B* **250,** 2431–2436 (2013).
29. Brychta, R. J., Shiavi, R., Robertson, D. & Diedrich, A. Spike detection in human muscle sympathetic nerve activity using the kurtosis of stationary wavelet transform coefficients. *J. Neurosci. Methods* **160,** 359–367 (2007).
30. te Velde, G. *et al.* Chemistry with ADF. *J. Comp. Chem.* **22,** 931–967 (2001).
31. Senthilkumar, K., Grozema, F. C., Bickelhaupt, F. M. & Siebbeles, L. D. A. Charge transport in columnar stacked triphenylenes: effects of conformational fluctuations on charge transfer integrals and site energies. *J. Chem. Phys.* **119,** 9809 (2003).
32. Martin, C. A., Smit, R. H. M., van Egmond, R., van der Zant, H. S. J. & van Ruitenbeek, J. M. A versatile low-temperature setup for the electrical characterization of single-molecule junctions. *Rev. Sci. Instrum.* **82,** 053907 (2011).
33. Kleinberg, J. in *Proc. 8th ACM SIGKDD Int. Conf. Knowledge Discovery and Data Mining* 91–101 (ACM, 2002).

Acknowledgements

The research leading to these results has received funding from the European Research Council (ERC) FP7 ERC Grant Agreement No. 240299 (Mols@Mols) and Horizon 2020 ERC Grant Agreement No. 648433.

Author contributions

N.R. and F.C.G. performed the electronic transport calculations and the molecular dynamics simulations. R.F., V.A.E.C.J. and H.S.J.Z. performed the break-junction experiments. R.F. designed and implemented the analysis of the plateaus. N.R. designed and implemented the higher-order statistical analysis of conductance drops. All the authors wrote the manuscript.

Additional information

Supplementary information is available in the online version of the paper. Reprints and permissions information is available online at www.nature.com/reprints. Correspondence and requests for materials should be addressed to F.C.G. and H.S.J.Z.

Competing financial interests

The authors declare no competing financial interests.